Nanostructure of HT-PEFC Electrodes Investigated with Scattering Methods

O. Holderer[a], M. Khaneft[a], Y. Lin[b], S. Liu[b], A. Feoktystov[a], M. Kruteva[c], R. Zorn[c], and W. Lehnert[b,d]

[a] Forschungszentrum Jülich, Jülich Centre for Neutron Science (JCNS) at MLZ, 85747 Garching, Germany
[b] Forschungszentrum Jülich, Institute of Energy and Climate Research (IEK-3), 52425 Jülich, Germany
[c] Forschungszentrum Jülich, Jülich Centre for Neutron Science (JCNS-1), 52425 Jülich, Germany
[d] RWTH Aachen University, Faculty of Mechanical Engineering, 52062 Aachen, Germany

The nanostructure of the electrode layer of a HT-PEFC is studied with neutron and X-ray small-angle scattering techniques. The different contrasts of the two probes provide a view on different aspects of the electrode layer. In combination with contrast variation by H-D isotope exchange further insight into the distribution of the different components on length scales in the range of 1-100 nm is obtained. An outlook shows the perspectives of scattering techniques for studying proton diffusion in such heterogeneous materials.

Introduction

Small-angle scattering with X-rays (SAXS) and neutrons (SANS) is used as a powerful tool to investigate different components of fuel cells or even groups such as membrane electrode assemblies (MEAs) (1,2). In particular, the structure of electrode layers of High Temperature Polymer Electrolyte Fuel Cells (HT-PEFCs) is studied in this contribution with neutron and X-ray scattering (1,3). Figure 1 shows a schematic drawing of the HT-PEFC and the electrode layer under study in this contribution. While X-ray and neutron radiography measurements have been applied in the past to study MEAs and HT-PEFCs on larger length scales (4-6), small-angle scattering provides information of relevant structural properties at nanometer length scales. Electrode layers in different stages of preparation, pure and doped with different amounts of phosphoric acid are studied with SAXS, which reveals structural changes with the addition of phosphoric acid. Details of the phosphoric acid distribution and possible void distribution in electrode layers will be obtained with contrast variation experiments in small-angle neutron scattering, where the different parts of the sample can be highlighted by exchanging protons with deuterons (or hydrogen with heavy hydrogen), here in the phosphoric acid.

An outlook will point at the strength of quasielastic neutron scattering experiments to shed light on the proton diffusion on different length scales in the range of 0.1-10 nm, as a microscopic equivalent to the macroscopic conductivity (7,8), and it will address the question of what can be retrieved from a multicomponent system such as the different parts of a fuel cell.

Experiments

Samples

Electrode layers of HT-PEFCs have been prepared from a catalytic powder consisting of Pt nanoparticles and carbon black support (20wt% Pt) which as been put into solution and mixed with PTFE. This ink has been coated onto a gas diffusion layer (GDL) with a doctor blade technique. Details can be found in Reference (1).

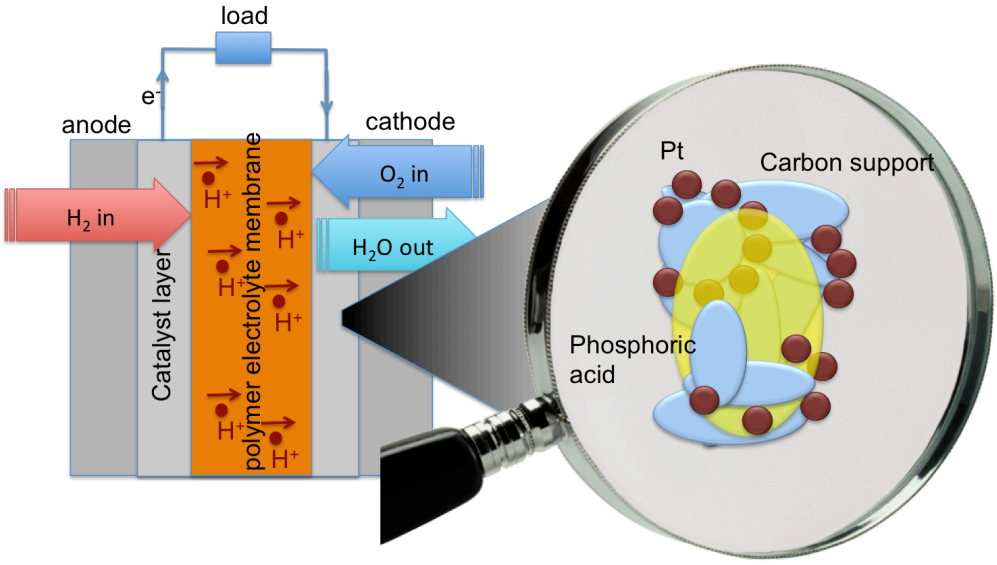

Figure 1: Schematic picture of a HT-PEFC with proton conducting membrane surrounded by the electrode layers. The zoom on the right shows a sketch of the electrode layer consisting of Pt catalyst particles on a carbon-PTFE support with phosphoric acid in the remaining space.

Neutron and X-ray scattering

Small-angle neutron scattering (SANS) is the method of choice for mesoscopic structures in the range of 1-100 nm, where light elements shall be investigated and where contrast variation by exchange of hydrogen (H) with heavy hydrogen (D) is possible. SANS provides an averaged image in Fourier space (i.e. spatial correlation functions). The characteristic length scales in the sample and shape information of objects can be deduced. SANS experiments have been conducted at the KWS-1 instrument at MLZ (Garching, Germany) (9, 10).

Similarly, small-angle X-ray scattering (SAXS) provides structural information on the same length scales but with a sensitivity proportional to the atomic weight Z of the components, i.e. the contrast increases for large differences in Z of the parts of the sample. The catalyst particles of the electrode embedded in the light matrix of carbon support are an example where SAXS can provide detailed information. SAXS experiments have been

performed at the GALAXI instrument at Forschungszentrum Jülich (11). The wavelength of the GaKα line used in this instrument is λ=1.34 Å.

Small-angle scattering results represent the scattered intensity as a function of the modulus of the reciprocal lattice vector, q.

Results and discussion

SAXS measurements on the electrode layer with different doping conditions (Figure 2) show the signature of the Pt catalyst particles having a radius of 1-2 nm at q~0.15 Å^{-1} (see also Ref (1)). At intermediate length scales (q=0.01 – 0.1 Å^{-1}) the curves follow a power law decay with a slope of -2, which is characteristic for disks formed by aggregation of Pt catalyst particles at the surface of the supporting carbon structure. An increase in phosphoric acid content seems to favor this slight rearrangement of the catalyst particles at the surface.

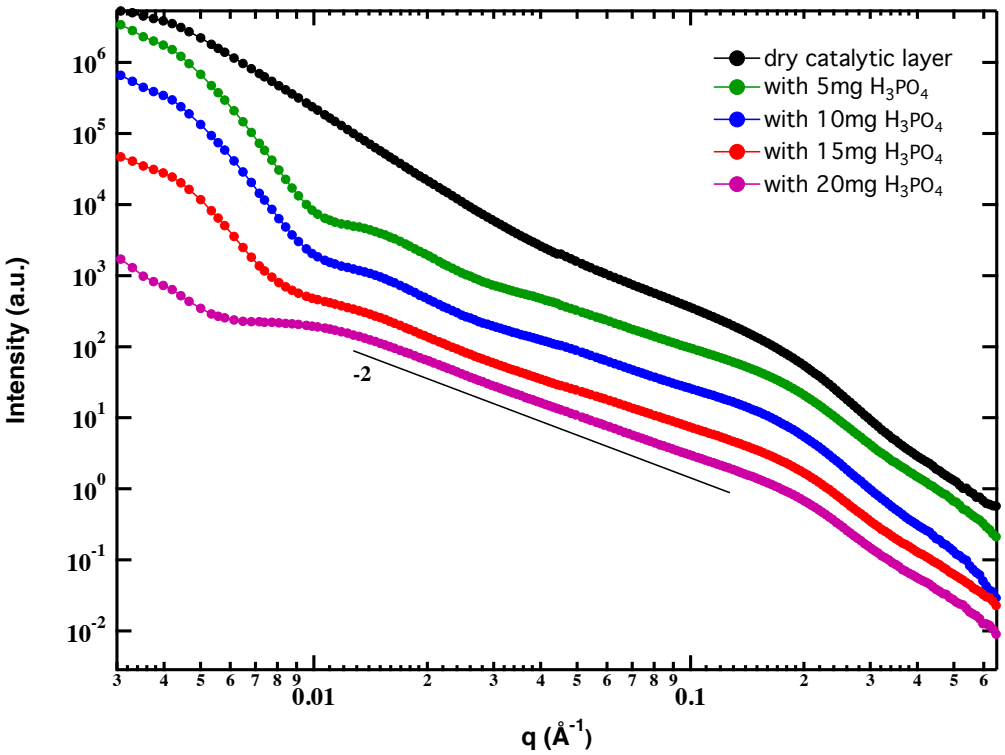

Figure 2: SAXS scattering curves of the catalyst layer with different amounts of phosphoric acid.

The evolution of the electrode layer upon first heating is shown in Figure 3. Filling the catalyst layer with phosphoric acid first of all results in a change in contrast, which is visible in a slightly changed scattering intensity at intermediate q.

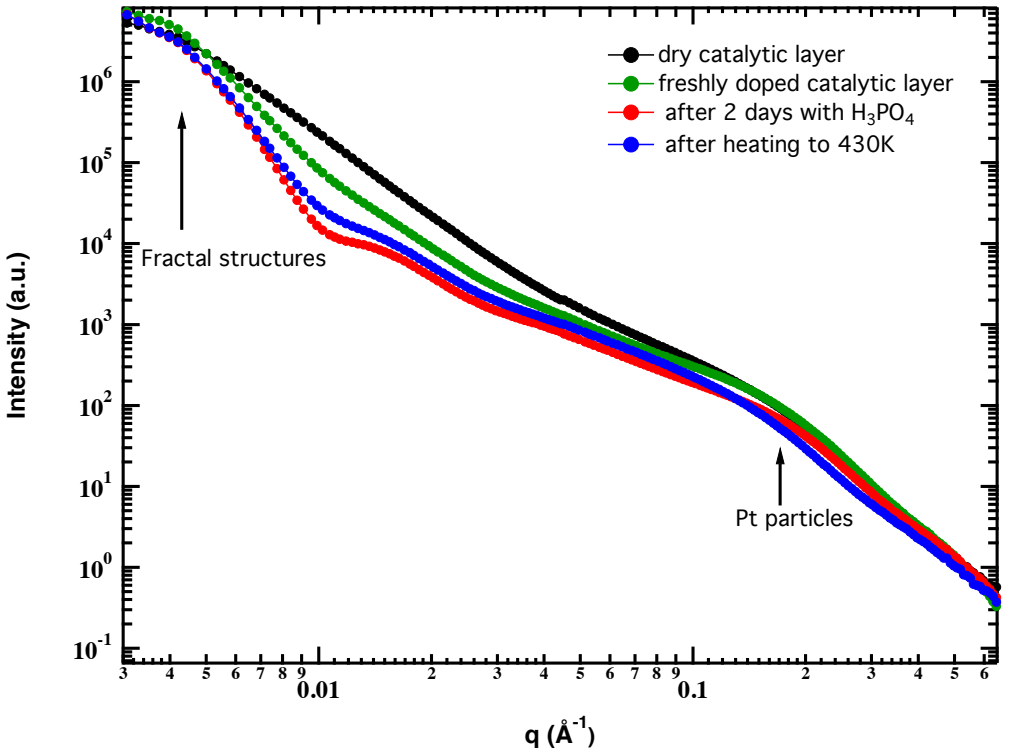

Figure 3: Structural evolution observed by SAXS from the dry layer to the first heating of the electrode.

The contrast in neutron scattering can be varied by the exchange of hydrogen (H) with heavy hydrogen (D), which have a largely different scattering cross section. It allows therefore to distinguish different components of the sample by contrast variation, e.g. in the present paper by varying the phosphoric acid composition from H_3PO_4 to D_3PO_4. The different scattering length densities (SLD) are listed in Table 1.

TABLE I. SLD's in the electrode layer

Component	SLD (10^{-6} Å^{-2})	Assumed Density (g/cm^3)
H_3PO_4 (85%)	1.9	1.88
D_3PO_4 (85%)	5.6	1.88
PTFE	4.8	2.2
Pt catalyst	6.2	21
Carbon support	6.7	2.0
Voids	0	0

Figure 4 shows SANS data from electrode layers. The strongest contrast in the case of a D_3PO_4-filled electrode layer would come from voids in the fractal structure of the electrode and catalyst particles, but there is also remaining contrast between carbon support, phosphoric acid and PTFE acting as a binder in the electrode layer. On the other hand, the higher the H_3PO_4 contents, the more the contrast between phosphoric acid and PTFE decreases. A strong difference in the SANS data is seen for the sample with 70% deuterated phosphoric acid which results in a SLD of about 4.5 x 10^{-6} Å^{-2}. At this condition it matches well the PTFE component, while in the other cases there are always contributions from the partial scattering cross sections between all components.

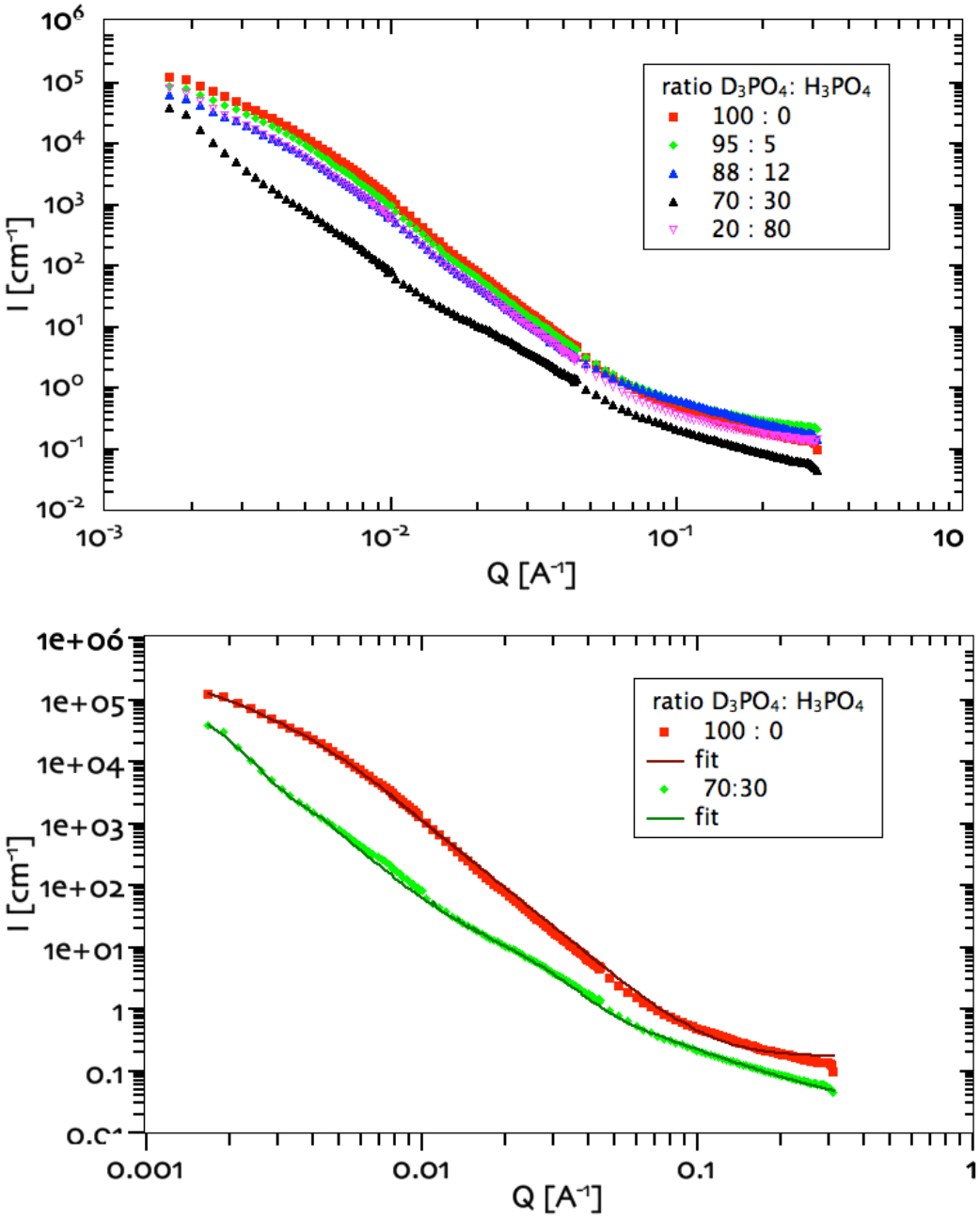

Figure 4: SANS scattering data for an electrode layer in different contrasts by varying the degree of deuteration of the phosphoric acid (top) and fitted data for the 100% deuterated phosphoric acid (dPA) doped sample compared with the 70% dPA.

Data have been fitted with the Beaucage model (12), an empirical model which combines an exponential fit (giving a characteristic length scale) with a power law fit of a fractal model (Fig. 4 lower part). The 100% dPA sample could be fitted with a single characteristic length scale of 82 nm and a power law exponent of -3.6 of a fractal structure, which contains in our opinion the many contributions from the different partial structure factors. In the case of 70% dPA we end up with much less visible components which reveals then some more relevant length scales in the sample. Carbon and Pt is one component, PTFE and phosphoric acid the second one, plus possible voids. The data could only be well described with 2 additional characteristic length scales (159 nm and 8

nm) which are probably caused by voids and the carbon structure on the near-uniform background SLD of phosphoric acid and PTFE. More details how to attribute the different components requires nonetheless further studies with a broader range of contrasts.

Conclusion

In this contribution we show how small-angle scattering with neutrons and X-rays (SAXS, SANS) can help to understand the structure of a complex multicomponent material such as the electrode layers. The different contrast situations allow drawing conclusions on the distribution of the different parts. Structural investigations are an important step towards the nanoscopic understanding of the electrode layers, but can be conducted further by quasielastic neutron scattering experiments (QENS), for example time-of-flight spectroscopy, backscattering spectroscopy or neutron spin-echo spectroscopy, all probing different time- and length-scales from sub-nm to some ~10 nm. With QENS, the proton transport mechanism can be studied on the same length scales as the structural investigations presented here which can help understanding the macroscopic relevant conductivity and link it with microscopic processes. Further studies will focus on this link between structure and transport.

Acknowledgments

Allocation of SANS beam time at the Heinz Maier-Leibnitz Zentrum (MLZ) in Garching is acknowledged.

References

1. M. Khaneft, O. Holderer, O. Ivanova, W. Lüke, E. Kentzinger, M.S. Appavou, R. Zorn, W. Lehnert, *Fuel Cells*, **16**, 406 (2016).
2. O. Ivanova, W. Lüke, A. Majerus, M. Krutyeva, N.K. Szekely, W. Pyckhout-Hintzen, M.-S. Appavou, M. Monkenbusch, R. Zorn, W. Lehnert, O. Holderer, *J. Mem. Sci.,* **533**, 342 (2017).
3. W. Lehnert, Ch. Wannek, R. Zeis, in Innovations in Fuel Cell Technology, R. Steinberger-Wilckens, W. Lehnert, Editors, p. 45 – 75, RSC Publishing, Cambridge (2010).
4. W. Maier, T. Arlt, K. Wippermann, C. Wannek, I. Manke, W. Lehnert, D. Stolten, *J. Electrochem. Soc.,* **159**, F398 (2012).
5. T. Arlt, W. Lüke, N. Kardjilov, J. Banhart, W. Lehnert, I. Manke, *J. Power Sources* **299**, 125 (2015).
6. P. Boillat, J. Biesdorf, P. Oberholzer, A. Kaestner, T. J. Schmidt, *J. Electrochem. Soc*. **161**, F192 (2014).
7. O. Holderer, O. Ivanova, B. Hopfenmüller, M. Zamponi, W. Maier, A. Majerus, W. Lehnert, M. Monkenbusch, R. Zorn, *Int. J. Hydrogen Energy* **39**, 21657 (2014).
8. O. Holderer, O. Ivanova, M. Khaneft, B. Hopfenmüller, W. Lüke, A. Majerus,

M.-S. Appavou, N.K. Szekely, M. Krutyeva, E. Kentzinger, R. Zorn, W. Lehnert, *ECS Transactions* **69**, 337 (2015).
9. H. Frielinghaus, A. Feoktystov, I. Berts, G. Mangiapia, *J. Large-Scale Research Facilities*, **1** A28 (2015).
10. A. V. Feoktystov, H. Frielinghaus, Z. Di, S. Jaksch, V. Pipich, M.-S. Appavou, E. Babcock, R. Hanslik, R. Engels, G. Kemmerling, H. Kleines, A. Ioffe, D. Richter and T. Brückel, *J. Appl. Crystallogr.,* **48**, 61 (2015).
11. E. Kentzinger, M. Krutyeva, U. Rücker, *J. Large-Scale Research Facilities*, **2**, A61 (2016).
12. B. Hammouda, *J. Appl. Crystallogr.,* **43**, 1474 (2010).